Two-color emitting colloidal nanocrystals as single particle ratiometric probes of intracellular pH

Francesco Bruni[1†], Jacopo Pedrini[1†], Caterina Bossio[2], Beatriz Santiago-Gonzalez[1], Francesco Meinardi[1], Wan Ki Bae[3], Victor I. Klimov[4], Guglielmo Lanzani[2,5*] and Sergio Brovelli[1*]

[1]*Dipartimento di Scienza dei Materiali, Università degli Studi di Milano-Bicocca, via Cozzi 55, IT-20125 Milano, Italy*

[2]*Center for Nano Science and Technology, Istituto Italiano di Tecnologia, Via Pascoli 70/3, 20133 Milano, Italy.*

[3]*Photo-Electronic Hybrids Research Center, National Agenda Research Division, Korea Institute of Science and Technology, Seongbuk gu, Seoul, Korea*

[4]*Chemistry Division, Los Alamos National Laboratory, Los Alamos, New Mexico 87545, United States*

[5] *Politecnico di Milano, Dip.to di Fisica, P.zza L. Da Vinci 32, 20133 Milano, Italy.*

[†] These authors contributed equally to this work.

(*) Correspondence should be addressed to Sergio Brovelli (sergio.brovelli@unimib.it) and Guglielmo Lanzani (guglielmo.lanzani@iit.it)

Intracellular pH is a key parameter in many biological mechanisms and cell metabolism. This parameter has been frequently used to detect and monitor cancer formation and brain or heart diseases. pH sensing is typically performed by fluorescence microscopy using pH responsive luminescent dyes. The accuracy of this method, however, is limited by the need for quantifying the absolute emission intensity of dye molecules in living biological samples. An alternative approach with a potentially much higher sensitivity and precision is based on probes with a ratiometric response arising from the different pH sensitivity of two emission channels of a single emitter. Current ratiometric probes are typically complex constructs consisting of inorganic nanostructures coupled to organic dyes, which suffer from poor photochemical stability and cross-readout due to the broad linewidths of their emission spectra. Here, we demonstrate that such limitations can be alleviated using a single-particle ratiometric pH probe based on fully inorganic dot-in-bulk CdSe/CdS nanocrystals (NCs). These nanostructures feature emission spectra comprising of two fully spectrally separated, narrow peaks with

markedly different pH sensitivity. These two emissions arise from radiative recombination of core- and shell-localized excitons, that are characterized by markedly different responses to the NC environment including the pH level. Specifically, the core emission is much less affected by the pH than the shell luminescence which undergoes drastic enhancement in the 3-11 pH range, resulting in a cross-readout-free ratiometric response as strong as 600%. In vitro microscopy of Human Embryonic Kidney cells demonstrates that the ratiometric response in biologic media closely resembles the pre-calibration curve obtained through far-field titration experiments. The NCs show good bio-compatibility, enabling us to monitor in real-time the externally induced pH variations in living cells.

Intracellular pH plays a fundamental role in the regulation of the cell metabolism and in a large number of biological mechanisms, such as glycolysis and hydrolysis of adenosine triphosphate (ATP), protein folding and enzyme activity.[1-4] Alterations of intracellular pH are also typically indicative of cancer [5-9] or major brain and heart diseases.[10-13] Sensing intracellular pH is, therefore, a key diagnostic tool in biological and medical sciences. Conventional intracellular fluorescent pH probes are organic fluorophores, whose luminescence is quenched in acidic or basic conditions, thus allowing monitoring the cellular pH. The most common organic dyes for pH sensing are fluorescines, cyanine derivatives[14-16] and, more recently, naphthalimide derivatives that feature multiple sites for target-specific functionalization.[17,18] Colloidal semiconductor nanocrystals (NCs)[19,20] and metal nanoclusters with biocompatible capping ligands[21] have been recently proposed as potential alternative materials for intracellular pH sensing,[22-25] as they combine high emission efficiency and size-tunable electronic properties with enhanced stability and exceptionally large surface-to-volume ratios. In addition, NCs feature broad, virtually continuous absorption spectra that allows for non-resonant excitation, which lowers the detection limit and boosts the contrast and the resolution of confocal microscopy by minimizing detrimental background signals due to the diffuse stray-light and the auto-fluorescence of organic tissues.[26-31] The biocompatibility of intracellular pH probes and their selectivity for specific cytoplasmic organelles can be further enhanced by using polymeric or silica nanoparticles or electrolyte nanocapsules as vehicles for their targeted internalization through the cellular membrane.[32-42]

A common experimental difficulty of radiometric luminescence pH sensing is that it requires the accurate quantitative estimation of the emission intensity in biological systems, which is typically strongly dependent on the concentration of fluorophores inside the cells and requires the use of fluorescent standards, such as rhodamines, to correct for the experimental conditions.[43] This is boosting the interest for ratiometric systems capable of reporting pH variation through the intensity ratio between two coexisting emissions with different pH sensitivity.[44-47] To date, ratiometric pH sensors are mostly based on metallic or semiconducting nanoparticles coupled to organic dyes, whose mutual photophysical interaction through charge- or energy-transfer is determined by the external environment, leading to pH-induced spectral variations.[48-52] Other proposed strategies comprise multi-component silica nanospheres[53] or polymeric vesicles embedding ratiometric organic sensors.[41] Despite the variety of proposed architectures, all ratiometric sensors available to date comprise of at least one organic component,[54-56] which typically suffer from low photostability. In addition to this, a common limitation of ratiometric pH sensors is the strong cross-readout due to the spectral overlap between the broad luminescence profiles of the two emitting species.[43]

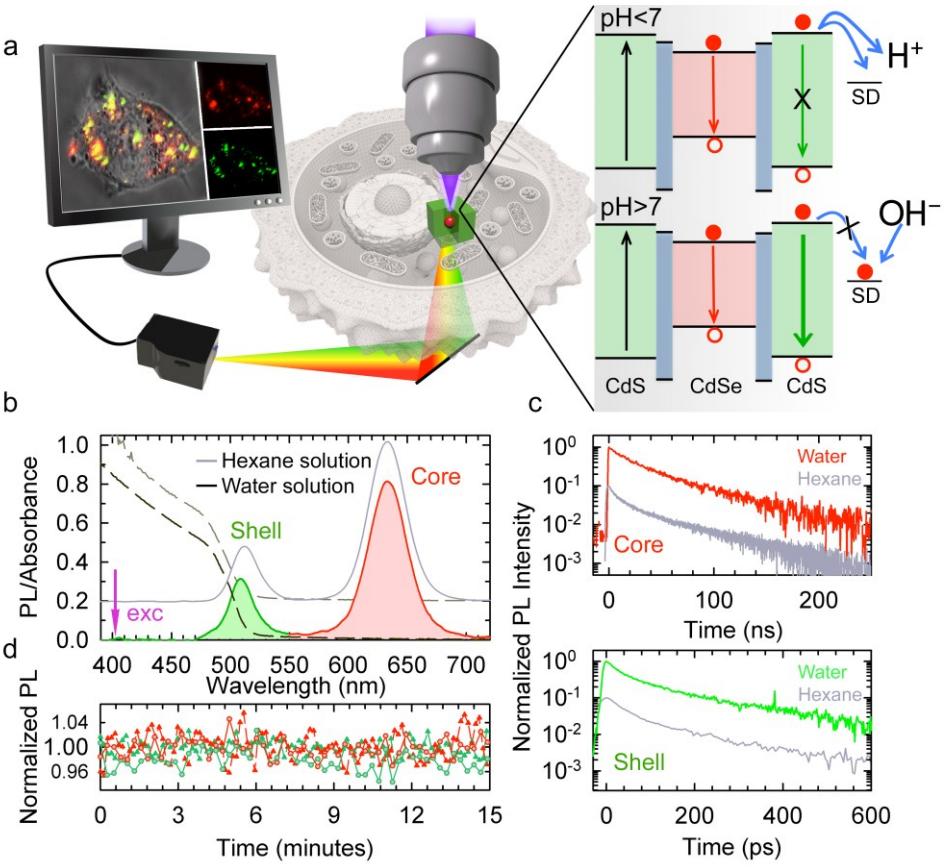

Figure 1. Concept of intracellular ratiometric pH sensing with Dot-in-Bulk NCs and optical properties. a. Schematic depiction of the use of two-color emitting DiB-NCs for intracellular pH ratiometric imaging, showing the simultaneous generation of two luminescence maps for the core and the shell emissions using the red and green detector channels of a confocal fluorescence microscope, respectively. The schematic representation of the band diagram of CdSe/CdS DiB-NCs and the pH sensing mechanism are shown in the right panel. At pH<7, excess H^+ cations quench the shell luminescence by directly removing electrons from the NC conduction band and by depleting (activating) electron accepting surface defects (SD). At pH>7, excess OH^- species passivate surface electron traps promoting the radiative recombination of excitons. **b.** Optical absorption (dashed lines) and photoluminescence (solid lines) spectra (λ_{EXC}=405 nm, excitation fluence 1μJ/cm^2) of as-synthesized CdSe/CdS DiB-NCs (core radius=1.5 nm, shell thickness=8.5 nm) capped with oleic acid in hexane (grey lines) and of the same NCs in water obtained through ligand exchange with thioglycolic acid molecules (black lines, pH=7). The absorption and emission spectra of the hexane NC solution have been rigidly shifted for clarity. The core and the shell emission bands in the spectra of aqueous NCs are highlighted by red and green shading, respectively. **c.** Comparison between the time decay curves of the core (upper panel) and the shell (lower panel) emissions of the two NC solutions, showing essentially identical recombination dynamics in water and in hexane. **d**. Normalized integrated PL intensity of the core (red curves) and the shell (green curves) emission under continuous illumination (λ_{EXC}=405 nm, excitation fluence 1μJ/cm^2) for thioglycolic-capped (triangles) and oleic acid passivated CdSe/CdS DIB-NCs in water and hexane respectively.

Here we show, for the first time, the use of intrinsically ratiometric two-colour emitting inorganic heterostructures as single-particle intracellular pH sensors, combining many important advantages over conventional pH probes. Namely, these systems are intrinsically ratiometric, which eliminates

the need for supramolecular constructs and for accurate control of secondary interactions and lifts the ubiquitous concentration-dependence of the response signal of radiometric pH probes. Equally importantly, our compact ratiometric nanostructures exhibit widely separated narrow-line emission bands, which completely suppresses cross-readout errors. Specifically, we use so-called dot-in-bulk CdSe/CdS NCs (DiB-NCs)[57-60] consisting of a small quantum confined CdSe core (radius ~1.5 nm) embedded in a bulk-like CdS particle (thickness ~8.5 nm). In Fig.S1a and Fig.S1b, we show transmission electron microscopy images of CdSe/CdS NCs during the synthesis at different shell thickness (3.5 nm and 8.5 nm respectively). Diffraction pattern collected at different reaction time show that the CdS shell grows in the same zincblende structure of the core for a few layers and then rearranges to the more thermodynamically stable wurtzite structure (Fig.S1c). As a result of their unique internal structure, featuring a sharp, unalloyed, core/shell interface[60] and a 30 meV potential barrier between the core and the shell valence bands[59] (Fig.1a), DiB-NCs exhibit two-color red and green emission respectively from core- and shell excitons under low fluence optical excitation (Fig.S2) or electrical drive.[57,59] Two-color light as a result of radiative recombination of excitons localized in different compositional domains of the same heterostructure has been observed also in elongated dot-in-rod structures, tetrapods[61-64] and spherical core/shell systems[65-70].

Representative photoluminescence (PL) spectra of DiB-NCs are reported in Fig.1b, showing the characteristic red and green emissions at 510 nm and 635 nm respectively. Fundamentally for ratiometric pH sensing, the core and shell excitons in DiB-NCs are differently exposed to the NC surfaces, which leads to a dramatically different response of their respective emission intensities to the local chemical environment:[57] the core PL is weakly affected by the surface chemistry, while suppression (activation) of electron trapping under negative (positive) electrochemical potentials leads to strong enhancement (quenching) of the green shell PL, resulting in a trajectory from red-to-yellow-to-green of the total emission colour as a function of the oxidative vs. reductive nature of the NC surroundings.[58] Furthermore, in DiB NCs, quenching of the shell PL is due exclusively to the extraction of photogenerated shell electrons, whereas holes photogenerated in the shell are unaffected by surface states and chemical agents due to their very short (~20-45 ps) residence time in the shell

states. As a result, DiB NCs are sensitive mostly to electron-withdrawing agents,[58] which makes them particularly suitable to optically probe the acidity of the NC surroundings and eliminates possible cross-sensitivity errors due to the competition between electron- and hole-trapping processes that characterize conventional core-only NCs. Thanks to this intrinsic ratiometric sensing ability, DiB-NCs have been very recently used to probe the local charge distribution at the interface between light-sensitive organic semiconductor thin films and water,[71] which constitute the functional platform of neural stimulation devices[72] for the realization of artificial retinal prosthesis for visual restoration.[73] These conditions resemble very closely the situation encountered in the pH sensing experiment schematically depicted in Fig.1a: H^+ ions act as electron scavengers resulting in a drop of the shell PL, while OH^- species saturate electron poor surface states, thus enhancing the shell emission intensity. As a result, we propose here an even more advanced application of DiB-NCs as intracellular ratiometric pH sensors whose response, in contrast to conventional ratiomeric pH probes, relies on the direct interaction between the photoexcited carriers and the local chemical surroundings.

The CdSe/CdS DiB-NCs were synthesized according to the procedure reported in ref.[59] using oleic acid as capping agent. To render the NCs soluble in water and thus compatible with bio-imaging experiments, we performed a ligand exchange procedure with thioglycolic acid.[74] The optical properties of DiB-NCs are fully preserved upon the ligand exchange procedure, as we report in Fig.1b, where we compare the optical absorption and PL spectra of a water solution of thioglycolic acid capped CdSe/CdS DiB-NCs and the analogous hexane solution of as-synthesized DiB-NCs capped with oleic acid. The organic and aqueous solutions show identical absorption spectra, with onset at ~520 nm due to strong absorption by the thick CdS shell, and PL profiles featuring two separated bands at 635 nm and 515 nm ascribed to the recombination of core and shell excitons, respectively.[59] The PL quantum efficiency of the pristine NCs (Φ_{PL}=14±2%) is also unchanged upon the ligand exchange procedure, as further confirmed by experimental quantum yield measurements and by the essentially identical decay dynamics of both the core (average lifetime $<\tau_C>$~35 ns) and shell ($<\tau_S>$~100 ps) emission in the two solvents reported in Fig.1c. In order to test the photostability of pristine and ligand exchanged NCs, we monitored their PL intensity for 15 minutes under

continuous illumination with UV light. The data in Fig.1d shows stable emission from the core and the shell for both the hexane and the water solution, thus confirming the stability of the NCs for illumination times significantly longer than the typical bio-imaging experiment. To further investigate the stability of the NCs, in Fig.S3 we report the same measurement performed over a period of 140 minutes showing good stability in the explored time range. Notably, the two-color emission of DiB-NCs is essentially independent of temperature in the 0-70°C range, as highlighted in Fig.S4 that shows a rigid red-shift of ~8 nm of both emission peaks and nearly constant I_S/I_C ratio and its first derivative $d(I_S/I_C)/dT$ across the whole temperature range. This is important for ratiometric pH sensing as it removes possible cross sensitivity effects due to variations of the sample temperature during the measurements.

To access the temporal stability of the DiB-NCs solution, we performed the titration measurement on a sample after 3 months of shelf time. The data show no evident aging effect on the NCs pH sensitivity (Fig.S6).

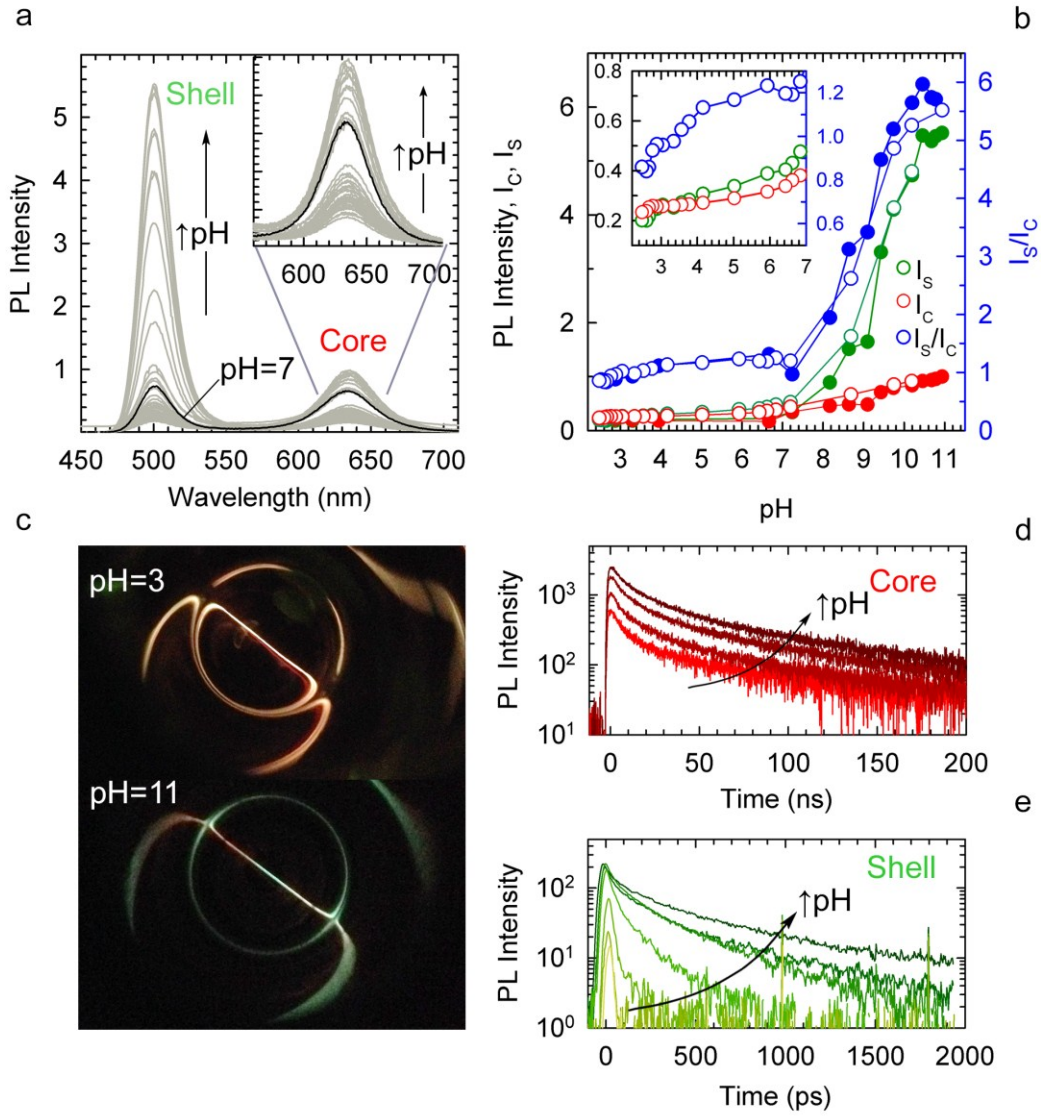

Figure 2. Demonstration of ratiometric pH sensing ability of DiB-NCs. a. Photoluminescence (PL) spectra of thioglycolic acid capped CdSe/CdS DiB-NCs in water at increasing pH (2-11) under 405 nm excitation (fluence 1 μJ cm^{-2}). The spectrum corresponding to the neutral condition (pH=7) is shown as a black line for reference. The inset shows a magnification of the core emission band as a function of the pH for clarity. **b.** Integrated intensity of the core (red circles, I_C) and the shell (green circles, I_S) emissions as a function of the pH in two consecutive cycles (full and empty circles) to demonstrate the reversibility of the pH sensing response. The ratio between the shell and core emission intensities (I_S/I_C) is reported as blue circles. The inset highlights the acidic pH range (one cycle only for clarity), showing a 2-fold variation of the ratiometric response. **c.** Top view photographs of the NC solution during the titration experiment at pH=3 (top panel) and pH=11 (lower panel) showing the dramatic change of total luminescence colour from red (dominated by the core emission) to green (dominated by the shell PL) upon increasing the solution pH. **d-e.** Normalized time decay curves of the core (red lines, λ_{PL}=635 nm) and the shell (green lines, λ_{PL}=500 nm) PL at increasing pH (as indicated by the arrow).

After assessing the stability of the DiB-NCs in polar environments, we proceeded with the demonstration of their ratiometric pH sensing ability. With this aim, we monitored the PL of DiB-NCs

in water as a function of the pH, which we controlled through titration with HNO_3 and NaOH under intense stirring. Optical absorption measurements of water suspensions of thioglycolic acid capped DiB-NCs, performed as a function of time at different values of pH and of the same NCs in KRH bicarbonate buffered saline solution containing magnesium, potassium, sodium and phosphate ions, demonstrate the excellent colloidal stability of the solution, showing no change in the absorption intensity and spectral profile in the investigated pH range (Fig.S5). Figure 2a displays a set of PL spectra for increasing pH from 2 to 11 recorded using c.w. excitation at 405 nm. In Figure 2b, we plot the amplitudes of the shell (I_S) and the core-related (I_C) PL bands extracted from the spectra together with their intensity ratio, I_S/I_C. The data shows the progressive growth of both emissions with increasing pH, which is ascribed to the progressive suppression of electron harvesting by H^+ ions upon basification of the solution (Fig.1a), in agreement with spectro-electrochemical observations in reductive conditions.[58] According to the direct exposure of shell excitons to the NC surfaces, I_S undergoes intense, ~30-fold, enhancement with increasing pH, which is almost 10 times stronger than the growth experienced by I_C in the same pH range (~4-fold increase). We notice that the same response is obtained in consecutive pH ramps (see filled dots in Fig.2b) and for thioglycolic acid capped DiB-NCs stored in air for three months (Fig.S6). As a result of this strong difference in pH sensitivity, I_S/I_C spans from 1 to 6 as a function of the pH with a major effect in the basic region (Fig.2b), leading to a progressive change of the total emission colour from red to green. This effect is highlighted in Fig.2c, where we report the photographs of the DiB-NCs solution at pH=3 and pH=11 under 400 nm laser excitation showing distinct red and green luminescence, respectively.

In order to gather deeper insight into the ratiometric sensing mechanism of DiB-NCs, we measured the time dynamics of both the core and the shell PL as a function of the pH. Looking first at the core emission in Fig.2d, we notice that the decay profile is essentially unaffected by the NC environment, whereas the zero-delay emission intensity grows with increasing pH. This indicates that the electron capture process responsible for PL quenching in acidic conditions is much faster than the ~ 1 ns resolution of the time-correlated single photon counter used for measuring the core PL dynamics. We note that, since the core excitons are localized away from the NC surfaces, extraction of core electrons

occurs in only a minor fraction of the NCs ensemble, whereas, in the majority of NCs, the core excitons are almost unaffected by the external conditions, leading to the mild sensitivity of the core PL of the local pH observed in the c.w. measurements. On the other hand, the inspection of the shell PL dynamics performed using a streak camera with ~5 ps resolution, reveals a strong effect of the pH on both the zero-delay PL intensity and on the shell exciton lifetime. This observation points to the coexistence of a distribution of electron capture processes occurring on different time regimes and affecting different subpopulations of NCs in the ensemble. The growth of the zero-delay signal confirms the ultrafast nature of the electron capture process observed for the core PL that, in a large portion of NCs in the ensemble, depletes the shell conduction band from photo-excited electrons before their radiative decay or localization into core states.[58] Concomitantly, the shell PL lifetime gradually increases upon basification, due to the progressive suppression of slower electron trapping processes, most likely associated to the distribution of NC-H^+ distances in water solution and with the variety of surface sites mediating the electron capture mechanism.[58]

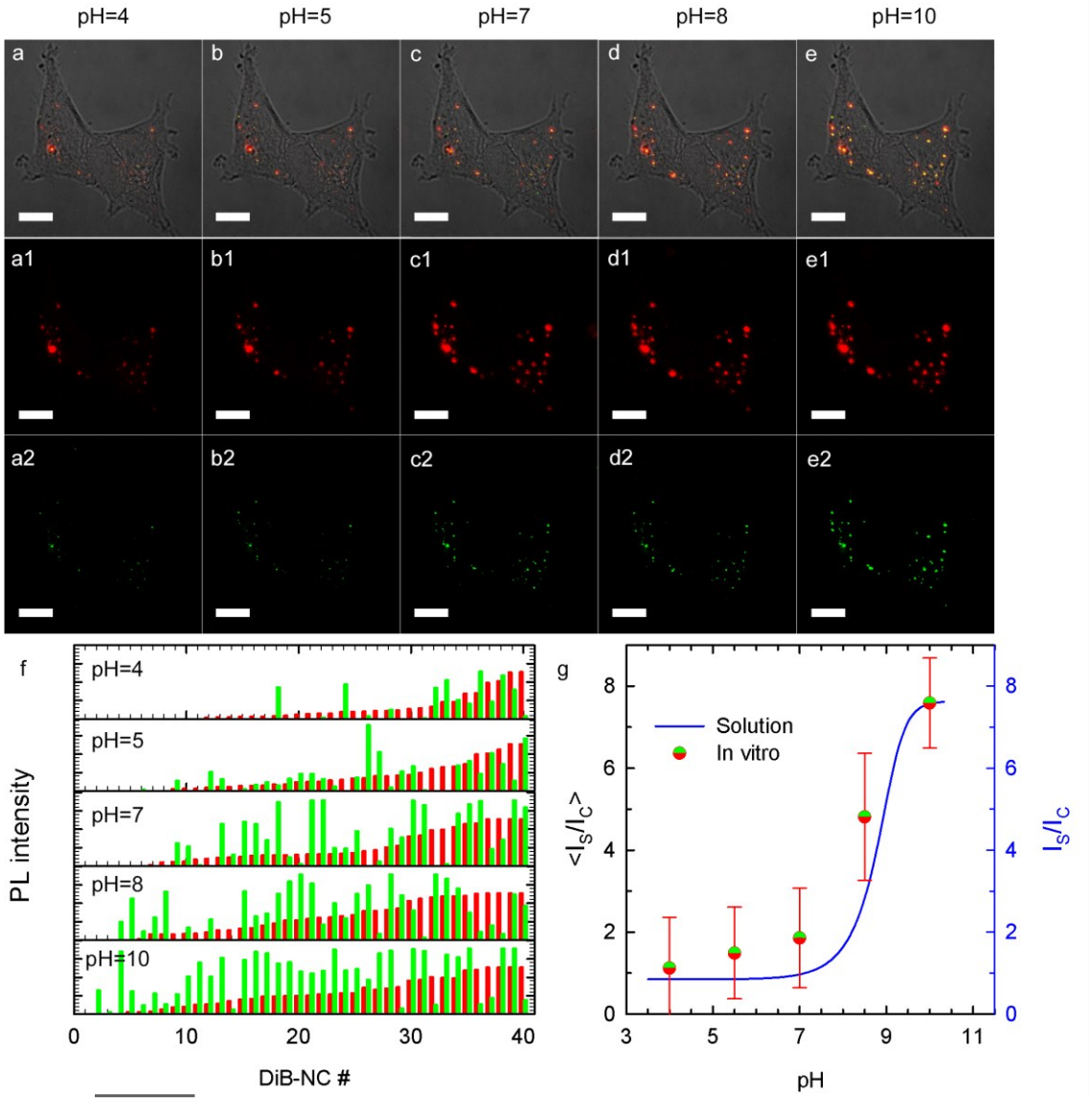

Figure 3 Intracellular pH sensing on fixed HEK-293 cells. Confocal images of HEK-293 cells stained with 130 nM DiB-NCs at increasing pH collected under 405 nm excitation (fluence 18 μJ cm^{-2}). **a-e.** Overlay of confocal images and bright-field images collected with a 60x, 1.4 NA, oil immersion objective. Evolution of the core (**a1-e1**) and shell (**a2-e2**) emission with increasing pH. The scale bar is 10μm for all panels. **f.** Histograms of shell (green bars) and core (red bars) PL intensity of the DiB-NCs collected selectively with the green and the red detector channels at increasing pH. **g.** Average shell-to-core PL intensity ratio ($\langle I_S/I_C \rangle$) as a function of the pH in fixed HEK-293 cells extracted from the histograms in '**f**' (circles). The ensemble I_S/I_C measured in aqueous solution is reported as a blue line.

To experimentally validate the ratiometric sensing ability of DiB-NCs in *in vitro* conditions, we internalized them into Human Embryonic Kidney (HEK-293) cells and monitored their PL as a function of the intracellular pH using confocal fluorescence microscopy. The time lapse imaging of NC internalization is shown in Fig.S8, together with the IC/IS ratio, showing progressive dimming of the shell PL for a

acidity of the cell membrane with respect to the culture medium. For fixed cells, the pH was changed by titrating the phosphate-buffered saline (PBS) solution with NaOH or HNO_3 solutions (0.1M) and each image of the same cell was recorded under identical excitation and collection conditions after 15 minutes from the addition of the titrating solution, so as to ensure the achievement of stable intracellular pH. In Fig.3 we report the fluorescence images of two HEK-293 cells stained with DiB-NCs overlaid to their respective bright field images (Fig.3a-e).

Because the DiB-NCs are not functionalized with target-specific ligands, they disperse inside the cell forming small domains of aggregated NCs, enabling us to visualize the local intracellular environment even at very low concentration. Better dispersion of the NCs inside the cell or their targeting to specific subcellular organelles is in principle achievable by suitable capping with site selective functionalities, which is however beyond the scope of this proof-of-principle study. In order to emphasize the ratiometric pH response of the DiB-NCs, in Fig.3a1-e1 and 3a2-e2, we report the fluorescence images collected using the red and green detector channels of the confocal microscope, so as to selectively monitor the evolution of the core and the shell PL, respectively. These set of images show the progressive emergence of the green shell luminescence for increasing pH (pH= 4-10) in agreement with the sensing behaviour observed in the ensemble measurements. The quantitative estimation of the ratiometric sensing response obtained by extracting the intensity of the two detection channels for 40 emitting spots as a function of the pH is reported in Fig.3f. In Fig.3g, we report the average ratiometric response $\langle I_S/I_C \rangle$ corresponding to the average pH response per detection spot, showing a similar trend as the ensemble response reported in Fig.2b. We notice that the differences between the absolute values of the ratiometric response in the confocal and far-field measurements is most likely due to the different optical configuration used in the two experiments and by the local inhomogeneity of the intracellular pH.

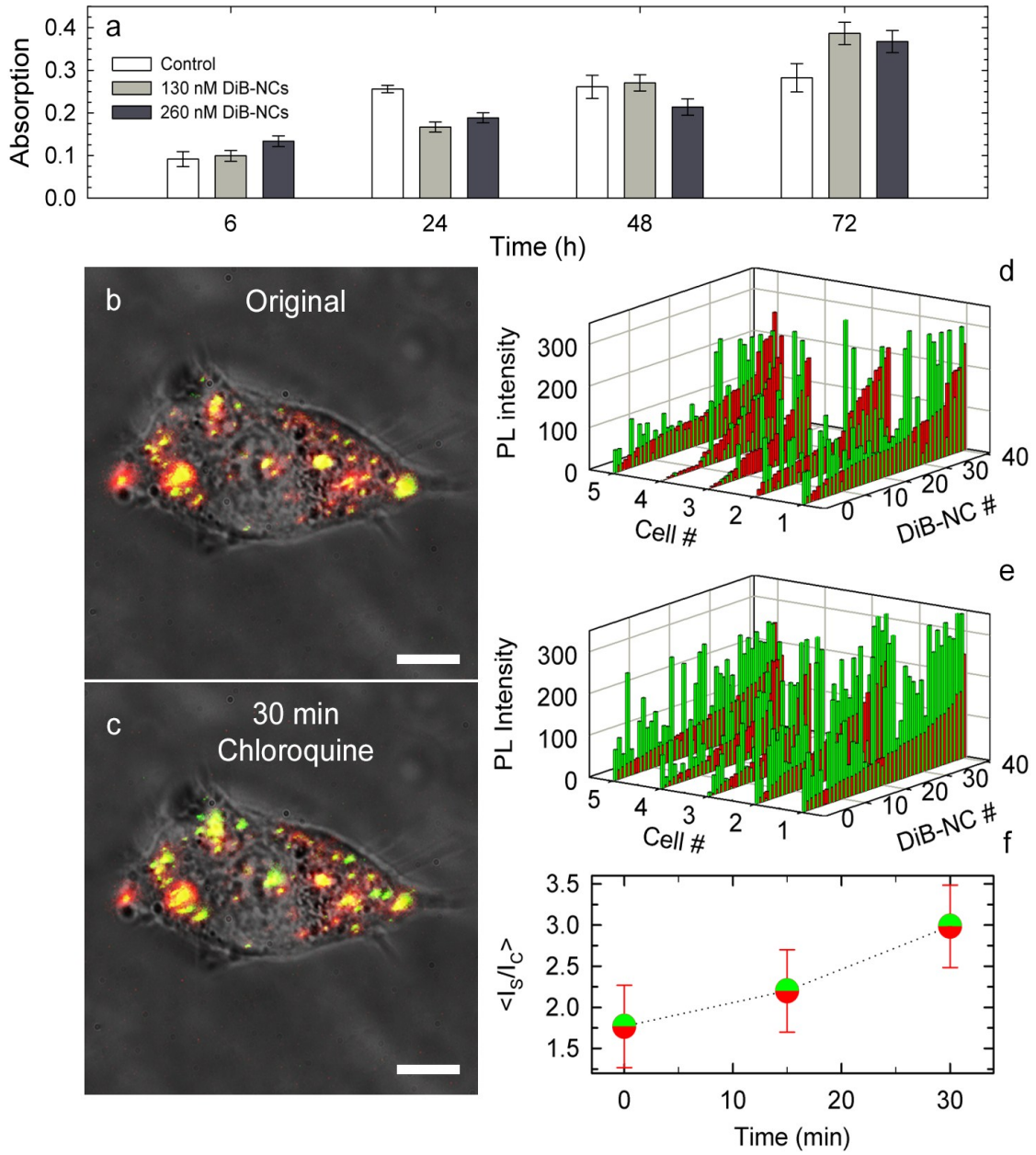

Figure 4 Cell proliferation experiments and intracellular ratiometric pH sensing in living HEK-293 cell. **a.** MTT test for cell viability up to 3 days in vitro for two different DiB-NCs concentrations (130 nM and 260 nM) and for untreated control cells (ctrl). Data are reported as average n = 12 ± SE. **b,c.** Overlay of confocal images collected with the red and green detector channel and bright-field images of living HEK cells stained with 130 nM DiB-NCs at increasing pH. The intracellular pH was modified by adding a 400 µf solution of chloroquine. The measurements were performed 30 min after adding the chloroquine solution. **d,e.** Histograms of green and red photoluminescence intensities for a statistically relevant ensemble of 40 NCs repeated for 5 different cell cultures. **f.** Average shell-to-core emission ratio as a function of exposure time to chloroquine extracted from the histograms in '**d,e'**.

We highlight, cell fixation preserves the tissues from degradation, but it terminates every biochemical process inside the cell, resulting in a different chemical environment with respect to that found in a

living sample.[75-79] To demonstrate that our approach is suitable for ratiometric intracellular pH sensing also in living cells, we therefore internalized DiB-NCs into HEK-293 cells in Krebs-Ringer Bicarbonate (KRH) buffer solution and induced changes in the intracellular pH by exposing the living cells to chloroquine, a weakly basic amine that accumulates into the lysosomes and into the Golgi apparatus, resulting in the basification of the intracellular environment.[80] Prior to the pH monitoring experiments, we evaluated the cytotoxicity of DiB-NCs by performing the MTT [3-(4,5-dimethylthiazol-2-yl)-2,5-diphenyltetrazolium bromide] assay on the HEK-293 cells after 6h, 24h, 48h and 72h of incubation with and without the NCs. MTT is reduced to formazan in living cells. Since this reduction depends on the cellular metabolic activity, stronger formazan optical absorption indicates progressively larger cell population.[81,82] Figure 4a shows the results of the MTT assay on cells stained with increasing concentrations of DiB-NCs, showing that cell proliferation is unaffected by the NCs, even at high concentration, which indicates good biocompatibility of DiB-NCs.

Based on these results, we proceeded with the pH measurements by exposing the cells to chloroquine. In Figure.4b and 4c, we show confocal images of a single living HEK cell stained with DiB-NCs before and 30 minutes after the exposure to a 400μM chloroquine solution,[83] overlaid to the respective bright field pictures. A first look at the confocal data reveals the significant brightening of the green shell PL upon addition of chloroquine, in agreement with its expected basification effect on the cell cytoplasm. To quantify the variation of the core and shell PL intensity and confirm the reproducibility of the pH sensing assay, in Fig.4d and 4e we report the histograms for 40 representative emitting spots for five different cells, showing the progressive enhancement of the shell emission with exposure time, whereas the core PL remains essentially unaltered by the addition of chloroquine. As a result, the $\langle I_S/I_C \rangle$ ratio increases almost by a factor of two for 30-minutes exposure (Fig.4f), thus confirming the suitability of our NCs as pH-sensitive optical probes for in-vitro applications.

In conclusion, we demonstrated the use of heterostructured NCs as intrinsic ratiometric probes for intracellular pH sensing. With this aim, we specifically chose CdSe/CdS DiB-NCs that show a

characteristic two-color emission arising from the simultaneous radiative recombination of core and shell excitons that are differently affected by the NC surfaces and chemical agents and can therefore be exploited to ratiometrically probe the local NC environment. This has been demonstrated through far-field spectroscopic measurements upon titration with HNO_3 and NaOH, leading to ~600% enhancement of the shell-to-core PL ratio and through confocal measurements on fixed and living HEK-293 cells in controlled pH conditions. Cell viability studies reveal good bio-compatibility of the DiB-NCs corroborating their potential as intracellular pH sensors. We note that the reported proof-of-principle CdSe/CdS NCs are not optimized in terms of the thickness of the CdS shell or the choice of the capping ligand and further improvements in the photoluminescence quantum efficiency and pH sensitivity might therefore be expected by optimizing the surface coverage and functionalization. The strategy demonstrated here for test-bed CdSe/CdS hetero-NCs is not composition specific and might, in principle, be extended to other semiconductors free from heavy metal elements, such as ternary I-III-VI_2 NCs,[84] as well as to heterostructures with different band alignment (type I, inverted type I etc…), so as to specifically tune the ratiometric response to acidic or basic conditions through selective exposure of holes or electrons to the intracellular environment.

Acknowledgements

Financial support from Fondazione Cariplo is acknowledged by S.B. and F.M. through grant No. 2012-0844). V.I.K. and W.K.B. were supported by the Chemical Sciences, Biosciences and Geosciences Division, Office of Basic Energy Sciences, Office of Science, U.S. Department of Energy. S.B. wishes to thank the European Community's Seventh Framework Programme (FP7/2007-2013) under grant agreement N. 324603 for financial support (EDONHIST).

Methods

Synthesis of CdSe/CdS DiB NCs

DiB NCs NCs were synthesized following the procedure described in ref.[57]. Briefly, zincblende CdSe NCs were synthesized by previously reported methods.[85] For the synthesis of CdSe (R_0 = 1.5 nm)/CdS NCs, 2×10^{-7}mol of CdSe NCs (purified twice) dispersed in 10 mL of 1-octadecene (ODE)

were loaded into a 100 mL flask, degassed at 110°C for 1 h. The flask was filled with Ar, and heated up to 300 °C for CdS shell growth. A 0.2 mmol sample of Cd-oleate and 0.2 mmol of 1-dodecanethiol were added slowly (0.1 mmol/min) and the reaction was maintained at the elevated temperature for 30 min to form a thin CdS buffer layer (~3 monolayers) on top of CdSe cores. For further CdS shell growth, a mixed solution of Cd-oleate and trioctylphospine-sulfur (0.5 M/0.5M) in ODE was continuously added at a rate of 1 mmol/hour at 300°C. After the injection of precursors was completed, the reaction products were cooled to room temperature and purified repeatedly by a precipitation-and-redispersion method. The final products were dispersed in hexane for further characterization.

Ligand exchange procedure

Hydrophobic NCs were transferred from organic solvent (hexane) to aqueous solution by adding thioglycol acid. Generally, an excess of thioglycol acid (twice the concentration of NCs), calculated according to ref.[74] was added to the hexane solution while stirring. After two hours, a solution of tetramethylammonium hydroxide having the same concentration as the thiol was added dropwise, rendering the NCs water soluble. The water phase was then separated and precipitated by adding isopropanol followed by centrifugation. (10 min at 5000 rpm). The precipitation was repeated twice redispersing then the pellet in ultrapure water.

Spectroscopic Studies

Optical absorption and emission measurements were performed on stirred NC solutions. Optical absorption spectra were measured with a Varian Cary 50 spectrophotometer. Steady-state and time-resolved photoluminescence (PL) spectra were excited by a frequency-doubled Ti:Sapphire laser (405 nm, pulse duration 150 fs, repetition rate 76 MHz). PL spectra were collected with a liquid-nitrogen cooled Instrument SA Spectrum One charge coupled device (CCD) coupled to a Horiba Scientific Triax 180 monochromator. The PL dynamics of shell emission in the sub-nanosecond time regime were measured with a Hamamatsu streak camera. The PL dynamics of core emission in the nanosecond time regime were studied with the same Ti:Sapphire laser as an excitation source but reducing its repetition rate to 760 kHz with a pulse picker based on a Conoptics 350-160 electro-optical modulator. The PL dynamics were measured with a Hamamatsu R943-02 time-correlated single-photon counting unit coupled to an Oriel Instruments Cornerstone 260 monochromator.

In the pH sensing measurements, the solution pH was modified by addition of 0.1M solutions of HNO_3 and NaOH and its value was monitored in situ using a Eutech XS pH6+ pH meter.

Cell Cultures HEK-293 cells were cultured in cell culture flasks containing Dulbecco's modified Eagle's medium (DMEM) with 10% Fetal Bovine Serum (FBS), 100 U ml-1 Penicillin, 100 µg ml-1 Streptomycin and 100 U ml-1 L-Glutamine. Culture flasks were maintained in a humidified incubator at 37 °C with 5% CO2. When at confluence, HEK-293 cells were enzymatically dispersed using trypsin-EDTA and then plated on the different polymer substrates at a concentration of 20,000 cells cm-2. Cells were fixed for 20 min at RT in 4% paraformaldehyde and 4% sucrose in 0.12 M sodium phosphate buffer, pH 7.4.

Cell proliferation (MTT assay)

In order to evaluate the cell viability with DiB-NCs, the MTT [3-(4,5-dimethylthiazol-2-yl)-2,5-diphenyltetrazolium bromide] (Sigma Aldrich) assay was performed on HEK-293 cells. Cells were seeded in 12 well plates at a density of 4x 10^4 cells/well with and without the DiB-NCs. Cell

proliferation was evaluated after 6 h, 24 h, 48 h and 72 h of incubation. For each time point, the growing medium was replaced with RPMI without phenol red containing 0.5 mg/mL of MTT. The samples were incubated again for 3 h at 37° C with 5% CO_2 in dark. Formazan salt produced by cells through reduction of MTT was then solubilized with 400 µL of ethanol and the absorbance was read at 560 nm and 690 nm. The proliferation cell rate was calculated as the difference in absorbed intensity at 560 nm and 690 nm.

KRH solution

The KRH solution contained [mM]: 135 NaCl, 5.4 KCl, 5 HEPES, 10 Glucose, 1.8 CaCl2, 1 MgCl2. pH 7.4

Confocal imaging studies

The sample cells were imaged with a Nikon C1 confocal microscope coupled with frequency-doubled Ti:Sapphire laser (405 nm, pulse duration 150 fs, repetition rate 76 MHz), with a 60x, 1.4 NA oil immersion objective. The spot diameter for this configuration is 350 nm. The green and red emission signals were collected selectively using the dedicated photomultiplier channel. The emission intensity was corrected for the respective spectral responses.

For fixed cells imaging, the cellular pH was changed by adding a Phosphate-Buffered Saline (PBS) solution at different pH. After each pH change we waited 15 minutes for the system to stabilize.

Living cells were observed while being kept in KRH 0.9 mM. The pH was changed by adding 100 µL of 4 mM chloroquine KRH solution, in order to obtain a 400 µM solution of chloroquine in the cellular environment. The excitation fluence was 48 µJ cm^{-2}.

References

1 Busa, W. B. & Nuccitelli, R. Metabolic regulation via intracellular pH. *Am. J. Physiol.* **246**, R409-438, (1984).

2 Casey, J. R., Grinstein, S. & Orlowski, J. Sensors and regulators of intracellular pH. *Nat. Rev. Mol. Cell. Biol.* **11**, 50-61, (2010).

3 Lagadic-Gossmann, D., Huc, L. & Lecureur, V. Alterations of intracellular pH homeostasis in apoptosis: origins and roles. *Cell Death Differ.* **11**, 953-961, (2004).

4 Wang, H. Y. & Oster, G. Energy transduction in the F-1 motor of ATP synthase. *Nature* **396**, 279-282, (1998).

5 Cardone, R. A., Casavola, V. & Reshkin, S. J. The role of disturbed pH dynamics and the Na+/H+ exchanger in metastasis. *Nat. Rev. Cancer.* **5**, 786-795, (2005).

6 Griffiths, J. R. Are cancer cells acidic? *Br. J. Cancer* **64**, 425-427, (1991).

7 Harguindey, S., Orive, G., Luis Pedraz, J., Paradiso, A. & Reshkin, S. J. The role of pH dynamics and the Na+/H+ antiporter in the etiopathogenesis and treatment of cancer. Two faces of the same coin--one single nature. *Biochim. Biophys. Acta* **1756**, 1-24, (2005).

8 Perona, R. & Serrano, R. Increased pH and tumorigenicity of fibroblasts expressing a yeast proton pump. *Nature* **334**, 438-440, (1988).

9 Tannock, I. F. & Rotin, D. Acid pH in Tumors and Its Potential for Therapeutic Exploitation. *Cancer Res.* **49**, 4373-4384, (1989).

10 Day, S. M. *et al.* Histidine button engineered into cardiac troponin I protects the ischemic and failing heart. *Nat. Med.* **12**, 181-189, (2006).

11 Obara, M., Szeliga, M. & Albrecht, J. Regulation of pH in the mammalian central nervous system under normal and pathological conditions: facts and hypotheses. *Neurochem. Int.* **52**, 905-919, (2008).

12 Sánchez-Armáss, S., Sennoune, S. R., Maiti, D., Ortega, F. & Martínez-Zaguilán, R. Spectral imaging microscopy demonstrates cytoplasmic pH oscillations in glial cells. *Am. J. Physiol.* **290**, C524-C538, (2006).

13 Vaughan-Jones, R. D., Spitzer, K. W. & Swietach, P. Intracellular pH regulation in heart. *J. Mol. Cell. Cardiol.* **46**, 318-331, (2009).

14 Hilderbrand, S. A., Kelly, K. A., Niedre, M. & Weissleder, R. Near Infrared Fluorescence-Based Bacteriophage Particles for Ratiometric pH Imaging. *Bioconjugate Chem.* **19**, 1635-1639, (2008).

15 Li, L., Li, Z., Shi, W., Li, X. & Ma, H. Sensitive and Selective Near-Infrared Fluorescent Off–On Probe and Its Application to Imaging Different Levels of β-Lactamase inStaphylococcus aureus. *Anal. Chem.* **86**, 6115-6120, (2014).

16 Tang, B. *et al.* A Near-Infrared Neutral pH Fluorescent Probe for Monitoring Minor pH Changes: Imaging in Living HepG2 and HL-7702 Cells. *J. Am. Chem. Soc.* **131**, 3016-3023, (2009).

17 Chen, L. *et al.* A novel pH "off-on" fluorescent probe for lysosome imaging. *RSC Adv.* **3**, 13412-13416, (2013).

18 Tian, Y. *et al.* A series of naphthalimide derivatives as intra and extracellular pH sensors. *Biomaterials* **31**, 7411-7422, (2010).

19 Pietryga, J. M. *et al.* Spectroscopic and Device Aspects of Nanocrystal Quantum Dots. *Chemical Reviews* **116**, 10513-10622, (2016).

20 Kovalenko, M. V. *et al.* Prospects of nanoscience with nanocrystals. *ACS nano* **9**, 1012-1057, (2015).

21 Boles, M. A., Ling, D., Hyeon, T. & Talapin, D. V. The surface science of nanocrystals. *Nat Mater* **15**, 141-153, (2016).

22 Gao, X. H., Chan, W. C. W. & Nie, S. M. Quantum-dot nanocrystals for ultrasensitive biological labeling and multicolor optical encoding. *J. Biomed. Opt.* **7**, 532-537, (2002).

23 Ji, X. *et al.* On the pH-Dependent Quenching of Quantum Dot Photoluminescence by Redox Active Dopamine. *J. Am. Chem. Soc.* **134**, 6006-6017, (2012).

24 Kaur, G. & Tripathi, S. K. Size tuning of MAA capped CdSe and CdSe/CdS quantum dots and their stability in different pH environments. *Mater. Chem. Phys.* **143**, 514-523, (2014).

25 Ma, J. *et al.* Photostability of thiol-capped CdTe quantum dots in living cells: the effect of photo-oxidation. *Nanotechnology* **17**, 2083-2089, (2006).

26 Deng, Z., Zhang, Y., Yue, J., Tang, F. & Wei, Q. Green and orange CdTe quantum dots as effective pH-sensitive fluorescent probes for dual simultaneous and independent detection of viruses. *J. Phys. Chem. B* **111**, 12024-12031, (2007).

27 Lakowicz, J. R. *Principles of fluorescence spectroscopy*. (Springer, 2010).

28 Maroto, A., Balasubramanian, K., Burghard, M. & Kern, K. Functionalized Metallic Carbon Nanotube Devices for pH Sensing. *ChemPhysChem* **8**, 220-223, (2007).

29 Medintz, I. L., Uyeda, H. T., Goldman, E. R. & Mattoussi, H. Quantum dot bioconjugates for imaging, labelling and sensing. *Nat. Mater.* **4**, 435-446, (2005).

30 Michalet, X. *et al.* Quantum Dots for Live Cells, in Vivo Imaging, and Diagnostics. *Science* **307**, 538-544, (2005).

31 Panda, B. R. & Chattopadhyay, A. A water-soluble polythiophene–Au nanoparticle composite for pH sensing. *J. Colloid Interface Sci.* **316**, 962-967, (2007).

32 Allard, E. & Larpent, C. Core-shell type dually fluorescent polymer nanoparticles for ratiometric pH-sensing. *J. Polym. Sci. A Polym.* **46**, 6206-6213, (2008).

33 Burns, A., Ow, H. & Wiesner, U. Fluorescent core-shell silica nanoparticles: towards "Lab on a Particle" architectures for nanobiotechnology. *Chem. Soc. Rev.* **35**, 1028, (2006).

34 Burns, A., Sengupta, P., Zedayko, T., Baird, B. & Wiesner, U. Core/Shell Fluorescent Silica Nanoparticles for Chemical Sensing: Towards Single-Particle Laboratories. *Small* **2**, 723-726, (2006).

35 Chen, Y.-N. *et al.* One-pot synthesis of fluorescent BSA–Ce/Au nanoclusters as ratiometric pH probes. *Chem. Commun.* **50**, 8571, (2014).

36 Peng, H.-s., Stolwijk, J. A., Sun, L.-N., Wegener, J. & Wolfbeis, O. S. A Nanogel for Ratiometric Fluorescent Sensing of Intracellular pH Values. *Angew. Chem. Int. Ed.* **49**, 4246-4249, (2010).

37 Wang, X.-d., Meier, R. J. & Wolfbeis, O. S. A Fluorophore-Doped Polymer Nanomaterial for Referenced Imaging of pH and Temperature with Sub-Micrometer Resolution. *Adv. Funct. Mater.* **22**, 4202-4207, (2012).

38 Hartmann, R., Weidenbach, M., Neubauer, M., Fery, A. & Parak, W. J. Stiffness-dependent in vitro uptake and lysosomal acidification of colloidal particles. *Angewandte Chemie* **54**, 1365-1368, (2015).

39 Clark, H. A. *et al.* Subcellular optochemical nanobiosensors: probes encapsulated by biologically localised embedding (PEBBLEs). *Sensors and Actuators B: Chemical* **51**, 12-16, (1998).

40 Gil, P. R., Nazarenus, M., Ashraf, S. & Parak, W. J. pH-sensitive capsules as intracellular optical reporters for monitoring lysosomal pH changes upon stimulation. *Small* **8**, 943-948, (2012).

41 Kreft, O., Javier, A. M., Sukhorukov, G. B. & Parak, W. J. Polymer microcapsules as mobile local pH-sensors. *Journal of Materials Chemistry* **17**, 4471, (2007).

42 Kantner, K. *et al.* Particle-based optical sensing of intracellular ions at the example of calcium - what are the experimental pitfalls? *Small* **11**, 896-904, (2015).

43 Shi, W., Li, X. H. & Ma, H. M. Fluorescent probes and nanoparticles for intracellular sensing of pH values. *Methods Appl. Fluoresc.* **2**, (2014).

44 Chen, S. *et al.* Full-Range Intracellular pH Sensing by an Aggregation-Induced Emission-Active Two-Channel Ratiometric Fluorogen. *J. Am. Chem. Soc.* **135**, 4926-4929, (2013).

45 Miesenbock, G., De Angelis, D. A. & Rothman, J. E. Visualizing secretion and synaptic transmission with pH-sensitive green fluorescent proteins. *Nature* **394**, 192-195, (1998).

46 Niu, C.-G. *et al.* Fluorescence ratiometric pH sensor prepared from covalently immobilized porphyrin and benzothioxanthene. *Anal. Bioanal. Chem.* **383**, 349-357, (2005).

47 Venn, A. A. *et al.* Imaging intracellular pH in a reef coral and symbiotic anemone. *Proc. Natl. Acad. Sci.* **106**, 16574-16579, (2009).

48 Medintz, I. L. *et al.* Quantum-dot/dopamine bioconjugates function as redox coupled assemblies for in vitro and intracellular pH sensing. *Nat. Mater.* **9**, 676-684, (2010).

49 Paek, K., Yang, H., Lee, J., Park, J. & Kim, B. J. Efficient Colorimetric pH Sensor Based on Responsive Polymer–Quantum Dot Integrated Graphene Oxide. *ACS Nano*, (2014).

50 Snee, P. T. *et al.* A Ratiometric CdSe/ZnS Nanocrystal pH Sensor. *J. Am. Chem. Soc.* **128**, 13320-13321, (2006).

51 Suzuki, M., Husimi, Y., Komatsu, H., Suzuki, K. & Douglas, K. T. Quantum dot FRET Biosensors that respond to pH, to proteolytic or nucleolytic cleavage, to DNA synthesis, or to a multiplexing combination. *J. Am. Chem. Soc.* **130**, 5720-5725, (2008).

52 Tomasulo, M., Yildiz, I. & Raymo, F. M. pH-Sensitive quantum dots. *J. Phys. Chem. B* **110**, 3853-3855, (2006).

53 Wang, X., Boschetti, C., Ruedas-Rama, M. J., Tunnacliffe, A. & Hall, E. A. Ratiometric pH-dot ANSors. *Analyst* **135**, 1585-1591, (2010).

54 Dennis, A. M., Rhee, W. J., Sotto, D., Dublin, S. N. & Bao, G. Quantum Dot–Fluorescent Protein FRET Probes for Sensing Intracellular pH. *ACS Nano* **6**, 2917-2924, (2012).

55 Jin, T., Sasaki, A., Kinjo, M. & Miyazaki, J. A quantum dot-based ratiometric pH sensor. *Chem. Commun.* **46**, 2408, (2010).

56 Shi, W., Li, X. & Ma, H. A Tunable Ratiometric pH Sensor Based on Carbon Nanodots for the Quantitative Measurement of the Intracellular pH of Whole Cells. *Angew. Chem. Int. Ed.* **51**, 6432-6435, (2012).

57 Brovelli, S. *et al.* Dual-Color Electroluminescence from Dot-in-Bulk Nanocrystals. *Nano Lett.* **14**, 486-494, (2014).

58 Brovelli, S. *et al.* Electrochemical Control of Two-Color Emission from Colloidal Dot-in-Bulk Nanocrystals. *Nano Lett.* **14**, 3855-3863, (2014).

59 Galland, C. *et al.* Dynamic Hole Blockade Yields Two-Color Quantum and Classical Light from Dot-in-Bulk Nanocrystals. *Nano Lett.* **13**, 321-328, (2013).

60 Pinchetti, V. *et al.* Effect of Core/Shell Interface on Carrier Dynamics and Optical Gain Properties of Dual-Color Emitting CdSe/CdS Nanocrystals. *ACS Nano*, (2016).

61 Wong, J. I. *et al.* Dual Wavelength Electroluminescence from CdSe/CdS Tetrapods. *ACS Nano* **8**, 2873-2879, (2014).

62 Soni, U. *et al.* Simultaneous Type-I/Type-II Emission from CdSe/CdS/ZnSe Nano-Heterostructures. *ACS Nano* **8**, 113-123, (2014).

63 Lin, Q. *et al.* Design and Synthesis of Heterostructured Quantum Dots with Dual Emission in the Visible and Infrared. *ACS Nano* **9**, 539-547, (2015).

64 Liu, S., Borys, N. J., Sapra, S., Eychmüller, A. & Lupton, J. M. Localization and Dynamics of Long-Lived Excitations in Colloidal Semiconductor Nanocrystals with Dual Quantum Confinement. *ChemPhysChem* **16**, 1663-1669, (2015).

65 Battaglia, D., Blackman, B. & Peng, X. Coupled and decoupled dual quantum systems in one semiconductor nanocrystal. *J. Am. Chem. Soc.* **127**, 10889-10897, (2005).

66 Nizamoglu, S. *et al.* Dual-color emitting quantum-dot-quantum-well CdSe-ZnS heteronanocrystals hybridized on InGaN/GaN light emitting diodes for high-quality white light generation. *Applied Physics Letters* **92**, 113110, (2008).

67 Sapra, S., Mayilo, S., Klar, T. A., Rogach, A. L. & Feldmann, J. Bright White-Light Emission from Semiconductor Nanocrystals: by Chance and by Design. *Advanced Materials* **19**, 569-572, (2007).

68 Teitelboim, A. & Oron, D. Broadband Near-Infrared to Visible Upconversion in Quantum Dot–Quantum Well Heterostructures. *ACS Nano*, (2015).

69 Zhao, H., Vomiero, A. & Rosei, F. Ultrasensitive, Biocompatible, Self-Calibrating, Multiparametric Temperature Sensors. *Small* **11**, 5741-5746, (2015).

70 Zhao, H. *et al.* Dual emission in asymmetric "giant" PbS/CdS/CdS core/shell/shell quantum dots. *Nanoscale*, (2016).

71 Mosconi, E. *et al.* Surface Polarization Drives Photoinduced Charge Separation at the P3HT/Water Interface. *ACS Energy Letters* **1**, 454-463, (2016).

72 Ghezzi, D. *et al.* A hybrid bioorganic interface for neuronal photoactivation. *Nat Commun* **2**, 166, (2011).

73 Ghezzi, D. *et al.* A polymer optoelectronic interface restores light sensitivity in blind rat retinas. *Nat Photon* **7**, 400-406, (2013).

74 Yu, W. W., Qu, L., Guo, W. & Peng, X. Experimental Determination of the Extinction Coefficient of CdTe, CdSe, and CdS Nanocrystals. *Chem. Mater.* **15**, 2854-2860, (2003).

75 Fox, C. H., Johnson, F. B., Whiting, J. & Roller, P. P. Formaldehyde Fixation. *J. Histochem. Cytochem.* **33**, 845-853, (1985).

76 Mariani, M. M., Lampen, P., Popp, J., Wood, B. R. & Deckert, V. Impact of fixation on in vitro cell culture lines monitored with Raman spectroscopy. *Analyst* **134**, 1154-1161, (2009).

77 Meade, A. D. *et al.* Studies of chemical fixation effects in human cell lines using Raman microspectroscopy. *Anal. Bioanal. Chem.* **396**, 1781-1791, (2010).

78 Schnell, U., Dijk, F., Sjollema, K. A. & Giepmans, B. N. G. Immunolabeling artifacts and the need for live-cell imaging. *Nat. Methods* **9**, 152-158, (2012).

79 Williams, Y. *et al.* Comparison of three cell fixation methods for high content analysis assays using quantum dots. *J. Microsc.* **232**, 91-98, (2008).

80 Chudzik, J., Ohkuma, S. & Poole, B. The effects of basic substances and acidic ionophores on the digestion of exogenous and endogenous proteins in mouse peritoneal macrophages. *J. Cell. Biol.* **102**, 959-966, (1986).

81 Gerlier, D. & Thomasset, N. Use of MTT colorimetric assay to measure cell activation. *Journal of Immunological Methods* **94**, 57-63, (1986).

82 Mosmann, T. Rapid colorimetric assay for cellular growth and survival: Application to proliferation and cytotoxicity assays. *Journal of Immunological Methods* **65**, 55-63, (1983).

83 Liu, Y.-S. *et al.* pH-Sensitive Photoluminescence of CdSe/ZnSe/ZnS Quantum Dots in Human Ovarian Cancer Cells. *J. Phys. Chem. C* **111**, 2872-2878, (2007).

84 Kolny-Olesiak, J. & Weller, H. Synthesis and application of colloidal CuInS2 semiconductor nanocrystals. *ACS applied materials & interfaces* **5**, 12221-12237, (2013).

85 Yang, Y. A., Wu, H., Williams, K. R. & Cao, Y. C. Synthesis of CdSe and CdTe nanocrystals without precursor injection. *Angew. Chem. Int. Ed.* **44**, 6712-6715, (2005).

Intracellular pH is a key parameter in biological mechanisms and cell metabolism. We demonstrate single-particle ratiometric pH probes based on hetero-nanocrystals featuring two-color emission with different pH sensitivity. In-vitro microscopy demonstrates that the intra-cellular ratiometric response resembles the pre-calibration curve obtained through far-field experiments. The nanocrystals show good bio-compatibility, enabling us to monitor externally induced pH variations in living cells.